# Phase Equilibria of L-Valine/L-Leucine Solid Solutions

Masoud Sadeghi[1*], Vico Tenberg[1], Stephan Münzberg[1], Heike Lorenz[1] and Andreas Seidel-Morgenstern[1,2]

[1]*Max Planck Institute for Dynamics of Complex Technical Systems, Magdeburg, Germany*

[2]*Otto-von-Guericke-University Magdeburg, Institute of Process Engineering, Chair for Chemical Process Engineering, Magdeburg, Germany*

*Corresponding author: E-Mail: sadeghi@mpi-magdeburg.mpg.de, Tel: +493916110321

**Abstract**

Modeling and experimental determination of Solid Liquid Equilibria (SLE) and the related phase diagrams are challenging in the presence of solid solutions. In this work, the ternary phase diagram of L-valine/L-leucine in water is measured and theoretically modelled at 298.15 K. The two similar molecules, L-valine and L-leucine form solid solutions as confirmed by Powder X-Ray Diffraction (PXRD) experiments. In addition, the concentrations of both equilibrated phases are determined using High Performance Liquid Chromatography (HPLC). Non-idealities are described using Perturbed Chain-Statistical Associating Fluid Theory (PC-SAFT) and Non-Random Two-Liquid (NRTL) models for the liquid and solid phases, respectively. The models work well to describe the solubility curve, except some extreme points. Finally, a graphical separation method based on the Lippmann plot is derived and its potential use will be expanded for the separation of organic compounds forming solid solutions.

**Keywords:** Solid solutions; Phase diagrams; Crystallization; Amino acids; Lippmann plot

## 1. Introduction

Separation of biomolecules is a crucial part of industrial bioprocesses and its associated charges can reach up to ninety percent of the total manufacturing costs [1]. As an efficient and cost-effective procedure, crystallization is widely used in bio industry to produce highly purified products. Therefore, rational design of a crystallization process is very important in the life sciences industries. This is achieved *via* the model-based plans instead of empirical descriptions.

For the successful operation of a crystallization process, it is necessary to know the phase diagram of the components involved. This task is very time-consuming when the resulting solid phase is a solid solution instead of a pure crystalline compound. Moreover, it imposes a challenging separation task, since a single purification step does not yield a pure product. Therefore, a multistage crystallization process is needed to achieve high purities.

As building blocks of proteins, amino acids play a very important role for life [2]. They are also important for the food technology and production of drugs [3]. Therefore, their industrial production and purification is of great importance. As a cost-effective method, crystallization can be used to purify amino acids. In this regard, solubility and phase diagram of amino acid molecules should be known.

In the literature, solubility behaviour of binary amino acid/solvent are widely available and discussed [4-7]. There are also some works regarding the solubility measurements of amino acids in mixed solvent systems [8]. Empirical as well as semi empirical models such as Wilson [9], modified Wilson [10], NRTL [11] as well as predictive models based on UNIFAC [12, 13] are widely used to model the behavior of the amino acid systems. SAFT-based models are also used to calculate the solubility of the amino acids [14, 15]. In a recent work, the performance of the excess Gibbs energy ($G^E$) models are compared with PC-SAFT for the calculation of the solubility and an improved accuracy for the description of the system

behavior using PC-SAFT is reported [16]. In all of these works, a pure solid phase is in equilibrium with a mixed liquid phase. In such cases, all of the tie lines end up in one of the corners of the phase diagram. Hence, there is no need to deeply consider the solid phase in the thermodynamic calculations. Although characterization of the solid phase with respect to polymorphism is necessary, experimental efforts are also drastically reduced as the solid phase is pure. However, this is not the case for the mixed-crystal systems. The mutual effect of the presence of two amino acids on each other's solubility is regarded as "salting-in" or "salting-out" phenomena. In such two-amino acid systems, there is a probability that the solid phase that is in equilibrium with the liquid is a solid solution or an intermediate binary compound. Therefore, these systems need to be considered with much more care and effort relative to the systems containing just one amino acid.

There are only a few studies regarding the solubility behaviour of aqueous L-valine/L-leucine systems [17, 18]. Some of them considered the formation of the mixed solid phase in this system [18]. In the present work, we deeply investigate this system extending the previous experimental and theoretical efforts. This is a part of a bigger plan as we aim to separate this solid solution forming system in a pilot-plant crystallization unit using counter-current crystallizers. Hence, phase diagrams for the aqueous solutions of the aforementioned amino acids are measured and their rational description based on thermodynamic concepts is presented. Formation of solid solutions is confirmed using PXRD experiments and HPLC was used to measure the concentration of equilibrated phases. Finally, the Lippmann diagram, which is a widely used concept in the field of inorganic solid solutions (particularly mineral systems), is extended to organic solid solutions forming systems [19].

## 2. Experimental section

*2.1. Samples.* The chemicals which were used for the experiments are: ʟ-valine (CAS: 72-18-4, Iris Biotech GmbH), ʟ-leucine (CAS: 61-90-5, Iris Biotech GmbH) and water (deionized with a Millipore40 filter, Resistivity: 18.2 MΩ cm, total organic carbon (TOC): 3 ppb). Amino acids were used as received without further purification. Table 1 describes the chemicals that are used in this work.

Table 1. Description of the chemicals used in this work

| Material | CAS | Assay (stated) | Source | Molar mass (g/mol) |
|---|---|---|---|---|
| ʟ-valine | 72-18-4 | 98.8 % | Iris Biotech GmbH | 117.15 |
| ʟ-leucine | 61-90-5 | 100.3 % relative to reference | Iris Biotech GmbH | 131.17 |

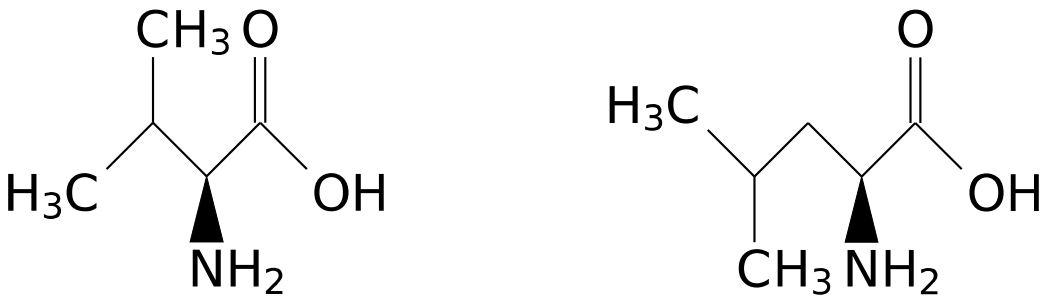


**Fig. 1.** Chemical structure of the amino acids ʟ-valine (left) and ʟ-leucine (right).

*2.2. Procedure.* For solubility measurements, desired amounts of ʟ-valine and ʟ-leucine mixtures at various compositions were dissolved in water. After complete dissolution was reached, the solution was transferred into a rotary evaporator. Then, the pressure was lowered towards a predefined boiling pressure, corresponding to the desired temperature, which was continuously monitored *via* a PT-100 resistance thermometer. The water was evaporated until significant crystal nucleation was observed. The dispersion was then transferred into a vial, which was sealed, stirred and kept at a desired temperature for at least 72 hours for complete equilibration between the liquid and solid phases. After equilibration, the liquid phase was sampled *via* a syringe filter. Then, the solid phase was separated using filter frits and dried in a vacuum oven at 313 K. Each phase composition was then determined *via* HPLC analysis.

For this, the samples were diluted using a two molar copper sulfate/methanol (90/10 vol. %) solution, which also acts as the eluent during the HPLC measurement. For the separation column, a Phenomenex Chirex® 3126 (D)-penicillamine column (length 50 mm, diameter 4.6 mm) is used for which 3 µL of a sample was injected at a flow rate of 0.5 mL $min^{-1}$. Using a pre-determined calibration line, the solubilities of the solid solutions in water and their corresponding solid phase composition were calculated. Additionally, the formation of solid solutions was verified by PXRD analysis of the solid phase. The PXRD analysis were performed on a PANalytical X'Pert Pro diffractometer in which the samples where measured using $Cu_{K\alpha}$ radiation in an angle of incidence ranging from 4 to 32° with a step size of 0.0167°. Each step was measured for 200 s.

**3. Theory**

Tie lines of the phase diagrams connect the composition of phases that are in equilibrium with each other. For systems showing solid solution behavior in the solid phase, multicomponent liquid and solid phases represent the two ends of the tie lines. Moreover, solid solutions forming systems may show alyotropic behavior similar to the azeotropic behavior in vapor-liquid systems. Fig. 2 shows a ternary phase diagram showcasing a typical tie line and the alyotropic behavior for a system consisting of a solvent and two solid solution forming solutes A and B. In the alyotropic systems a solubility maximum (or minimum), higher (or lower) than the respective pure component solubilities exist. The l-valine/l-leucine/water system shown in this work possesses a solubility maximum alyotrope. At the alyotropic point, the composition of the solid phase and the solvent free liquid phase are equal and therefore, the corresponding tie line is overlapping with an isopleth. Due to this, crystallization at the alyotropic composition does not enrich either solute in the corresponding phases.

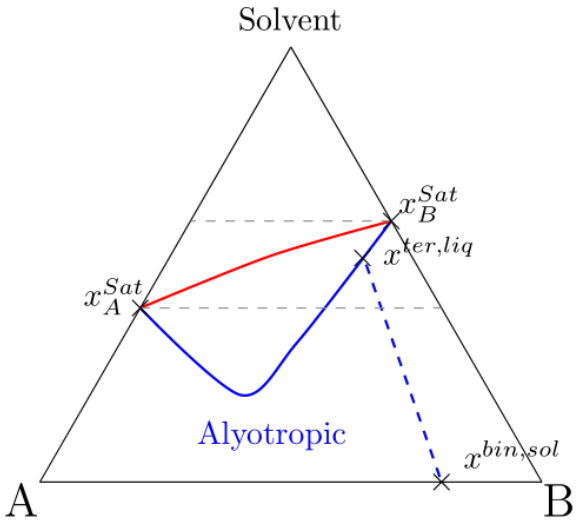


**Fig. 2.** Ternary phase diagram showcasing nonalyotropic (red) as well as alyotropic (blue) behavior in an arbitrary A-B-Solvent system.

Here, aqueous solutions of ʟ-valine and ʟ-leucine are in equilibrium with solvent-free solid solutions of the two amino acids. Hence, the fugacity of each amino acid *i* is equal in liquid and solid phases. Each of the fugacities can be expressed in terms of the activity coefficients $(\gamma)$, mole fractions $(x)$ and the reference state fugacities $(f^0)$:

$$x_i^{bin,sol}\gamma_i^{bin,sol}f_i^{0,sol}=x_i^{ter,liq}\gamma_i^{ter,liq}f_i^{0,liq} \quad .$$

(1)

Where superscripts bin, sol and ter, liq stand for binary solid and ternary liquid, respectively. Choosing the pure melt as the reference state, we may consider another equilibrium between a pure solid and a binary liquid solution at the same temperature as the binary solid solution. In this case, we find a relation between the reference fugacities as follows:

$$f_i^{0,sol}=x_i^{bin,liq.}\gamma_i^{bin,liq.}f_i^{0,liq} \quad .$$

(2)

Combination of *Eqs*. (1) and (2) leads to the following relation between the activity coefficients of the amino acids [18]:

$$x_i^{bin,sol}\gamma_i^{bin,sol}=\frac{x_i^{ter,liq}\gamma_i^{ter,liq}}{x_i^{bin,liq}\gamma_i^{bin,liq}} \quad .$$

(3)

Amino acids decompose before they melt. Using *Eq*. (3) enables us to model their behavior without knowing their melting information. It should be added that most of the amino acid molecules exist as zwitterions, positively charged or negatively charged species depending on the pH of the solution. As we consider the neutral pH, it is safe to neglect the effect of positively or negatively charged species. In fact, amino acids exist as zwitterions in the neutral pH. However, we consider amino acids as neutral molecules inside the thermodynamic modeling.

The activity coefficients of each component are the key properties required for an accurate description of the phase diagrams. In this work, PC-SAFT equation of state (EoS) [20] and NRTL equation [21] are used to describe the non-idealities of the liquid and solid phases, respectively. In what follows, we briefly introduce these models and information that is more detailed can be found in the respective publications [20-22].

*3.1. PC-SAFT EoS*

PC-SAFT is a theory-based EoS that considers the molecules like the chains of connected spherical segments. These chains interact with each other *via* chain, dispersion or associating forces. In this model, each species is described *via* physically sound component-specific parameters. Hence, each component is described using segment number $(m)$ , segment diameter $(\sigma)$ and dispersion energy $\left(\frac{u}{k}\right)$ parameters. For the components with hydrogen bonding ability, two other parameters should be considered. These are association energy $\left(\frac{\varepsilon^{A_i B_i}}{k}\right)$ and association volume $\left(\kappa^{A_i B_i}\right)$ parameters. In total, each component can

potentially be described using five adjustable parameters. Therefore, the compressibility factor is written as:

$$Z = 1 + Z^{hard\,chain} + Z^{dispersion} + Z^{association} \quad (4)$$

The expressions for each hard chain $\left(Z^{hard\,chain}\right)$ , dispersion $\left(Z^{dispersion}\right)$ , and association $\left(Z^{association}\right)$ contributions can be found in the literature [20, 22]. Extension of this model to the mixtures will be straightforward using mixing rules [20, 23]:

$$\left(\frac{u}{k}\right)_{ij} = \left(1 - k_{ij}\right)\sqrt{\left(\frac{u}{k}\right)_{ii}\left(\frac{u}{k}\right)_{jj}} \quad (5)$$

$$\sigma_{ij} = \frac{\sigma_{ii} + \sigma_{jj}}{2} \quad (6)$$

$$\frac{\varepsilon^{A_i B_j}}{k} = 0.5\left(\frac{\varepsilon^{A_i B_i}}{k} + \frac{\varepsilon^{A_j B_j}}{k}\right) \quad (7)$$

$$\kappa^{A_i B_j} = \left(\frac{\sqrt{\sigma_{ii}\sigma_{jj}}}{\sigma_{ij}}\right)^3 \sqrt{\kappa^{A_i B_i}\kappa^{A_j B_j}} \quad (8)$$

Here, $k_{ij}$ is adjusted to correct for the geometric mean assumption in the dispersion energy term.

*3.2. NRTL model*

NRTL explicitly considers the concentration and temperature dependence of the activity coefficients, which we use to calculate the activity coefficients in the solid phase. For a typical solute B in a binary solution AB, NRTL reads as [24]:

$$\ln\left(\gamma_B\right) = x_A^2\left[\tau_{AB}\left(\frac{g_{AB}}{x_B + x_A g_{AB}}\right)^2 + \frac{g_{BA}\tau_{BA}}{\left(x_A + x_B g_{BA}\right)^2}\right] \quad (9)$$

$$g_{AB} = \exp\left(-\alpha\tau_{AB}\right) \quad (10)$$

$$g_{BA} = \exp\left(-\alpha\tau_{BA}\right) \quad (11)$$

$$\tau_{AB}=\frac{b_{AB}}{RT}(12)$$

$$\tau_{BA}=\frac{b_{BA}}{RT}(13)$$

The adjustable parameters $(b_{AB},b_{BA})$ and the non-randomness parameter $(\alpha)$ could be obtained by fitting the model to the experimental data.

**4. Lippmann plot**

Total solubility product is a concept widely used in the field of mineralogy and was presented by Lippmann for minerals forming solid solutions [25]. He introduced the solutus and solidus lines in analogy with dew and bubble point curves of *p-x-y* diagrams in the field of vapour-liquid equilibria (VLE). This concept is widely used in geosciences dealing with solubility behaviour of the minerals. Here we suggest using this concept for the organic compounds that form solid solutions. To begin, we consider a binary solid solution (here it is composed of ʟ-valine and ʟ-leucine) which is in equilibrium with a ternary liquid phase (aqueous solution of ʟ-valine and ʟ-leucine). Therefore, the liquid and solid phase chemical potentials of each compound are equal and *Eq*. (1) holds. We rearrange *Eq*. (1) and show the ratio of standard fugacities by character *K*:

$$x_i^{sol}\gamma_i^{sol}\frac{f_i^{0,sol}}{f_i^{0,liq}}=x_i^{liq}\gamma_i^{liq},\frac{f_i^{0,sol}}{f_i^{0,liq}}=K_i \quad .$$

(14)

The reader should note that $K_i$ does not depend on concentration and is a characteristic of the pure $i$ at the system temperature. We may write *Eq*. (14) for each of ʟ-valine and ʟ-leucine. Hence, the total solubility product $\left(\sum K_{eq}\right)$ is defined as follows [19, 25]:

$$\sum K_{eq}=x_{val}^{liq}\gamma_{val}^{liq}+x_{leu}^{liq}\gamma_{leu}^{liq}=K_{val}\,x_{val}^{sol}\gamma_{val}^{sol}+K_{leu}\,x_{leu}^{sol}\gamma_{leu}^{sol} \quad .$$

(15)

In addition, the activity fraction $\left(X_{val}^{liq}\right)$ is represented for both ʟ-valine and ʟ-leucine [19]:

$$X_{val}^{liq}=\frac{x_{val}^{liq}\gamma_{val}^{liq}}{x_{val}^{liq}\gamma_{val}^{liq}+x_{leu}^{liq}\gamma_{leu}^{liq}} \quad .$$

(16)

$$X_{leu}^{liq}=\frac{x_{leu}^{liq}\gamma_{leu}^{liq}}{x_{val}^{liq}\gamma_{val}^{liq}+x_{leu}^{liq}\gamma_{leu}^{liq}} \quad .$$

(17)

We rearrange *Eq*. (14) and use *Eq*s. (16) and (17) to have expressions for the mole fractions of ʟ-valine and ʟ-leucine in the solid phase:

$$x_{val}^{sol}=\frac{x_{val}^{liq}\gamma_{val}^{liq}}{K_{val}\gamma_{val}^{sol}}=\frac{X_{val}^{liq}\left(x_{val}^{liq}\gamma_{val}^{liq}+x_{leu}^{liq}\gamma_{leu}^{liq}\right)}{K_{val}\gamma_{val}^{sol}} \quad .$$

(18)

$$x_{leu}^{sol}=\frac{x_{leu}^{liq}\gamma_{leu}^{liq}}{K_{leu}\gamma_{leu}^{sol}}=\frac{X_{leu}^{liq}\left(x_{val}^{liq}\gamma_{val}^{liq}+x_{leu}^{liq}\gamma_{leu}^{liq}\right)}{K_{leu}\gamma_{leu}^{sol}} \quad .$$

(19)

We realize that inside the parenthesis of *Eq*s. (18) and (19) is by definition, the total solubility product. Moreover, mass balances hold for the phases, for the solid phase this yields:

$$x_{val}^{sol}+x_{leu}^{sol}=\frac{X_{val}^{liq}\left(\sum K_{eq}\right)}{K_{val}\gamma_{val}^{sol}}+\frac{X_{leu}^{liq}\left(\sum K_{eq}\right)}{K_{leu}\gamma_{leu}^{sol}}=1 \quad .$$

(20)

Rearranging *Eq*. (20) gives a relation for $\sum K_{eq}$ *vs*. $X_{val}^{liq}$ which is called the solutus line by Lippmann [19, 25]:

$$\sum K_{eq}=\frac{1}{\frac{X_{val}^{liq}}{K_{val}\gamma_{val}^{sol}}+\frac{X_{leu}^{liq}}{K_{leu}\gamma_{leu}^{sol}}}=\frac{1}{\frac{X_{val}^{liq}}{K_{val}\gamma_{val}^{sol}}+\frac{1-X_{val}^{liq}}{K_{leu}\gamma_{leu}^{sol}}} \quad .$$

(21)

This relation resembles the dew point calculation of VLE. On the other hand, *Eq*. (15) is a relation for $\sum K_{eq}$ *vs*. $x_{val}^{sol}$ which represents the solidus line [19, 25]. This is in analogy with the bubble point calculations of the VLE. Having both of *Eq*s. (15) and (20) gives us the so-called Lippmann plot [19, 25], in which we have the solutus and solidus lines in the same diagram. Note that, the solutus line relates $\sum K_{eq}$ to the activity fraction in the liquid phase, while the solidus line relates $\sum K_{eq}$ to the mole fraction of the solid phase. Hence,

we should superimpose two scales on the abscissa of the diagram [19]. This is possible as both $x_{val}^{sol}$ and $X_{val}^{liq}$ vary between 0 and 1.

## 5. Results and discussion

In this work, two similar solutes exist in the liquid phase and they can crystallize in a common lattice, forming solid solutions. Except few studies [18], the formation of solid solution in this system is mostly ignored. However, our results confirm that for the aqueous solution of L-valine and L-leucine, solid solutions are formed and they need to be considered for the construction of a proper phase diagram. Fig. 3 shows the PXRD diagrams of the solid phases obtained from the solubility measurements. As this figure shows, the X-ray patterns gradually change from pure L-valine pattern to pure L-leucine pattern. Especially, the peaks in the range of 6 to 7.5° and 12 to 14° clearly display this gradual change usually connected with a continuous change in the corresponding lattice parameters. This is the case, when a solid solution is present in the solid phase instead of pure or intermediate compounds [26, 27]. It should be added that the PXRD diagram shows angles up to 32 degrees since the specific peaks of both pure components as well as their solid solutions can be seen in this range and analyzing further angles does not yield more information. Moreover, in particular peaks around 20 and 25 degrees may indicate another compound. We are investigating this intermediate compound in an ongoing work.

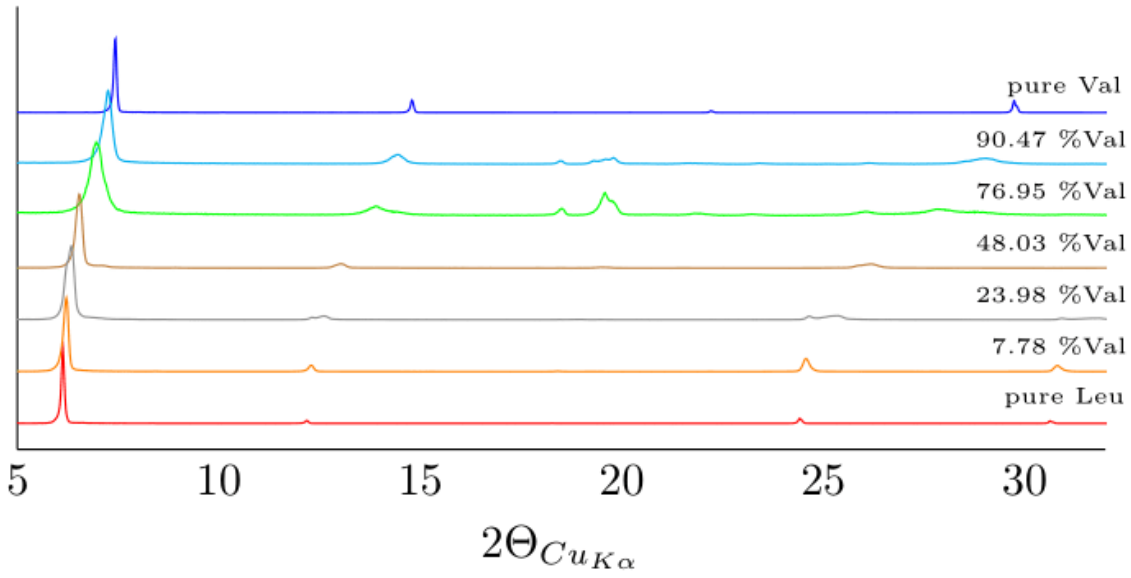


**Fig. 3.** PXRD patterns of various L-leucine - L-valine mixtures showing a gradual change of pure L-valine pattern to pure L-leucine pattern that is a distinctive behavior of a solid solution forming system. The compositions are mass percents of L-valine.

As this is a metastable phase, it is not considered in our equilibrium calculations although it may affect our experimental data to some extent. Parallel to PXRD measurements, HPLC analysis was performed to calculate the composition of equilibrated liquid and solid phases. The resulting solid and liquid molar fractions of L-valine and L-leucine can be found in Table 2. As this table shows, aqueous solubility of L-valine is nearly three times higher than for L-leucine at 298.15 K. L-leucine is a bigger molecule, having more non-polar functional groups (Fig. 1); therefore, it is less soluble than L-valine. This information can be displayed in a ternary phase diagram as shown in Fig. 4. Addition of L-valine to the pure aqueous L-leucine system, increases its solubility and we observe the so-called “salting-in” effect. On the other hand, addition of the L-leucine increases the solubility of L-valine. However, the solubility curve passes through a solubility maximum, which is an alyotropic point. At this point, the composition of the solid and liquid are the same on a solvent-free basis. Also, the tie line overlaps with the respective isopleth limiting the crystallization process.

Table 2. Liquid and solid molar fractions for L-valine and L-leucine in water determined at 298.15 K and their activity coefficients calculated using PC-SAFT and NRLT for the liquid and solid phases, respectively.

| $x_{l-val}^{liq}$ | $x_{l-leu}^{liq}$ | $\gamma_{l-val}^{liq}$ | $\gamma_{l-leu}^{liq}$ | $x_{l-val}^{sol}$ | $x_{l-leu}^{sol}$ | $\gamma_{l-val}^{sol}$ | $\gamma_{l-leu}^{sol}$ |
|---|---|---|---|---|---|---|---|
| 0.0093 | 0.0000 | 0.0600 | 0.1450 | 1.0000 | 0.0000 | 1.0000 | 4.7736 |
| 0.0119 | 0.0012 | 0.0604 | 0.1459 | 0.8922 | 0.1078 | 1.0135 | 3.7935 |
| 0.0128 | 0.0018 | 0.0604 | 0.1459 | 0.7125 | 0.2875 | 1.1169 | 2.5766 |
| 0.0113 | 0.0023 | 0.0602 | 0.1453 | 0.3664 | 0.6336 | 1.9785 | 1.3509 |
| 0.0087 | 0.0028 | 0.0599 | 0.1447 | 0.2346 | 0.7654 | 2.9408 | 1.1404 |
| 0.0057 | 0.0031 | 0.0589 | 0.1419 | 0.1170 | 0.8830 | 4.6440 | 1.0351 |
| 0.0042 | 0.0031 | 0.0587 | 0.1413 | 0.1052 | 0.8948 | 4.8892 | 1.0284 |
| 0.0009 | 0.0031 | 0.0557 | 0.1330 | 0.0163 | 0.9837 | 7.4859 | 1.0007 |
| 0.0000 | 0.0031 | 0.0548 | 0.1306 | 0.0000 | 1.0000 | 8.1528 | 1.0000 |

Standard uncertainties u are u($T$) = 0.2 K and u($x$) = 0.0001 (for 0.95 level of confidence).

All of the experimental information including the formation of solid solutions should be considered in the phase equilibrium calculations. As the solid phase is not pure, we need to consider the activity coefficients in the solid phase in addition to the non-idealities of the liquid phase. Therefore, implicit *Eq*. (3) should be written and solved for both L-valine and L-leucine simultaneously. In this equation, PC-SAFT is used to calculate the activity coefficients of the solutes in the liquid phase. All of the pure component as well as the interaction parameters are taken from the literature [15] and in this sense; the calculation is pure prediction. There is no reliable model to describe the activity coefficients in the solid phase. Apart from empirical models, local composition models may be assumed to work also for the solid phase for the correlation of the data. We use NRTL that is widely used in the field of VLE to describe the activity coefficients of the solid phase. Therefore, both of the PC-SAFT and NRTL models are used to simultaneously consider the nonidealities of the liquid and solid phases. Based on these models, rational activity coefficients in the liquid and solid phases are calculated and given in Table 2. Activity coefficient values in most cases deviate from the Raoult's law, showing the highly non-ideal behavior in both phases. The liquid phase activity coefficients are less than one, showing a negative deviation from Raoult's law. However, the activity coefficients in the solid phase are greater than one and show positive deviations from Raoult's law. All of the parameters of the models are presented

in Tables 3 and 4, respectively. The values shown in Table 3 are fitted to experimental data and should therefore be seen as just empirical parameters as opposed to physical parameters.

Having models to capture the activity coefficients, implicit Eq. 3 should be solved for both L-valine and L-leucine to construct their aqueous solubility line. Eq. 3 shows an implicit relation between mole fraction of the amino acid in the liquid phase ( $x_i^{ter,liq}$ ) and the mole fraction of the amino acid in the solid phase ( $x_i^{bin,sol}$ ). The curve of the upper part in Fig. 4 is the locus of all of $x_i^{ter,liq}$ points in the phase diagram. $x_i^{bin,sol}$ consist the other side of the tie lines on the lower edge of the triangular phase diagram.

As Fig. 4 shows, the solubility curve can be described applying the current models. However, tie lines around the solubility maximum cannot be calculated properly.

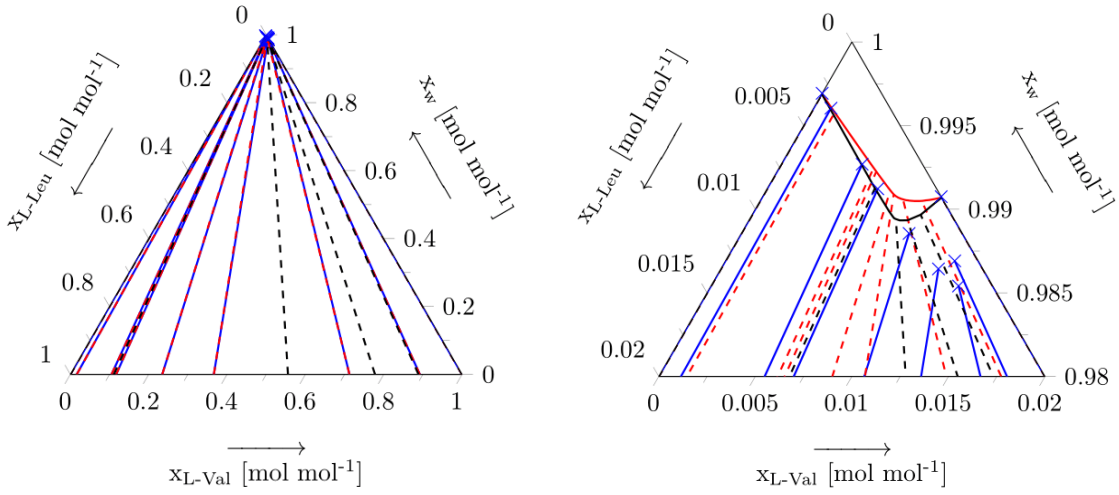


**Fig. 4.** Ternary phase diagram of L-valine and L-leucine in water. Left: complete ternary phase diagram. Right: zoomed view to enhance visibility. Experimental data (—, blue), model data (---) with predictive PC-SAFT (red) and with fitted $k_{ij}$ parameters (black).

Table 3. NRTL-parameter fitted to experimental data in this work

| $b_{l-val,l-leu}$ (- | $b_{l-leu,l-val}$ (- | $\alpha$ |
|---|---|---|
| 3294632.28 | -3228689.34 | 1.43E-5 |

Table 4. Component-specific parameter and values of $k_{ij}$ used in this work.

| Component | $m$ | $\sigma(A)$ | $\frac{u}{k}$( $K$ | $\frac{\varepsilon^{A_i B_i}}{k}$( | $\kappa^{A_i B_i}$ | $k_{ij}(H_2O)_{25}$ | $k_{ij}(H_2O$ | Ref |
|---|---|---|---|---|---|---|---|---|
| L-Valine | 7.4851 | 2.5888 | 306.41 | 3183.80 | 0.0385 | -0.0757 | 3.85E-4 | [15] |
| L-Leucine | 8.3037 | 2.7000 | 330.00 | 3600.00 | 0.0200 | -0.0630 | 4.09E-4 | [15] |
| Water | 1.2047 | * | 353.94 | 2425.67 | 0.0451 | 0.0000 | 0.0000 | [28] |

*: $\sigma = 2.7927 + 10.11 \cdot \exp(-0.01775 \cdot T) - 1.417 \cdot \exp(-0.01146 \cdot T)$

For a better description of the solubility curve, we tried to fit the binary interaction parameter of the PC-SAFT to the experimental data. As Fig. 4 shows, this method slightly improves the description of the experimental data; however, solubility maximum cannot be described adequately. Our goal is to describe the experimental data using the minimal adjustable parameters and the results show that more work is needed to describe such a complex behavior. To look more closely at the data, the Roozeboom diagram is constructed as a valuable tool for designing *e.g.* a counter-current crystallization process [29]. It is represented in Fig. 5 and shows that the system has an alyotrope in the higher L-valine concentration region where the equilibrium curve crosses the 45 ° line.

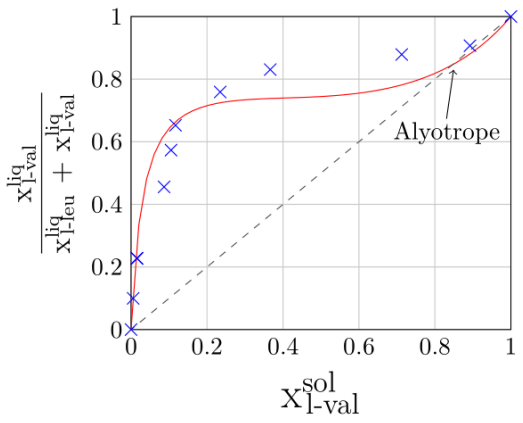


**Fig. 5.** Roozeboom type phase diagram: L-valine mole fraction in the solid phase as a function of solvent free L-valine mole fraction in the liquid phase. Red line is calculated using PC-SAFT and NRLT.

We add that the experimental data in Fig. 4 more explicitly supports the existence of an alyotrope and this information is more visible through the modelled data in Fig. 5.

Looking in a different way, we propose to construct a Lippmann diagram for this system. To confirm the alyotrope, Fig. 6 shows the proposed Lippmann diagram for the L-valine / L-leucine /water system for a constant temperature of 298.15 K. The reader should note that

in a Lippmann diagram, the activity fraction in the liquid phase plays a role and the effect of the activity coefficients are considered. In this figure, the total solubility product is plotted against the solid phase mole fraction that is called the solidus line. In addition, total solubility product *vs*. activity fraction in the liquid phase forms the solutus line. This figure is similar to a minimum azeotrope in an isothermal *p-x-y* diagram for VLE. Lippmann plot can be used for the design of the crystallizers in a similar way that *p-x-y* diagrams are used for the design of distillation columns. The information of the Lippmann plot can be transferred to a Roozeboom diagram, as shown in Fig. 7. This is again similar to transferring the information of a *p-x-y* diagram to the *x-y* plot.

To acquire a proper match of the alyotrope, the solid molar fraction needs to be plotted against the activity fraction in the Roozeboom diagram as well. Therefore, for this system Roozeboom type and the Lippmann diagram show the alyotropic point similar to an azeotropic point of a typical *p-x-y* diagram. Apparently, the position of the alyotrope in Fig. 5 does not match the depiction in Figs. 6 and 7. The reader should note that in Fig. 5 two mole fractions are used while in Figs. 6 and 7 we use the activity fraction for the liquid phase, which contains the effect of the activity coefficients. Therefore, there is no discrepancy between the diagrams, it is only written in two different languages.

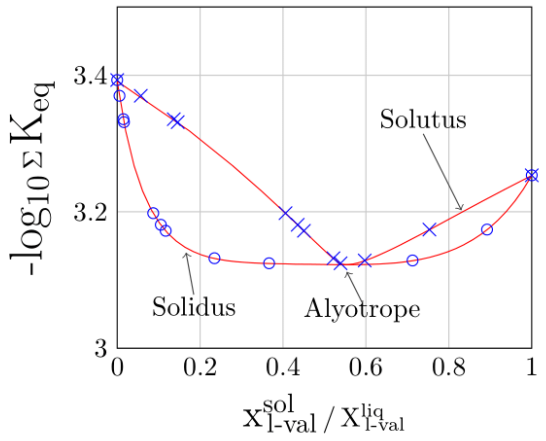


**Fig. 6.** Lippmann plot that is total solubility product as a function of L-valine mole fraction in the solid or activity fraction in the liquid phase. Red lines are calculated using PC-SAFT and NRTL models and

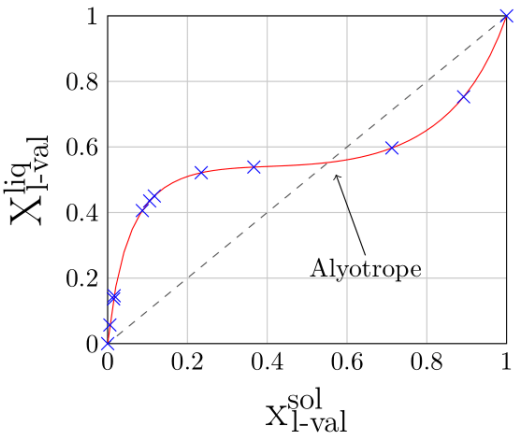


**Fig. 7.** Calculated (lines, red) and experimental (crosses, blue) in a Roozeboom type phase diagram: L-valine activity fraction in the liquid phase as a function of L-valine mole fraction in the

points are obtained using experimental data. solid phase

Nevertheless, the Lippmann plot and its associated Roozeboom diagram are valuable tools to design crystallization processes and we suggest using such diagrams for the separation of organic molecules, which form solid solutions.

## 6. Conclusions and outlook

A rational description of solid solutions forming systems is presented and applied to the case of the L-valine / L-leucine /water system. The activity coefficients of the species in the liquid and solid phases are taken into account using PC-SAFT and NRTL models, respectively. The results show that both liquid and solid phases behave nonideal and the activity coefficients deviate from unity in the sense of Raoult's law. L-valine is roughly three times more soluble than L-leucine in water and their solid solutions have a specific solubility behavior. In this system a solubility maximum exists which corresponds to an alyotrope. At this point, a tie line and an isopleth overlap with each other and further purification is not possible using conventional crystallization processes. Our modeling strategy gave reasonable agreement between the calculated and the experimental data for the solubility curve and its tie lines towards the edges of the ternary phase diagram. However, the models fail to accurately represent the solubility maximum in the system and tie lines near it. The concept of Lippmann diagrams is extended to the organic solid solutions forming systems. This valuable tool that considers the effect of activity coefficients can be efficiently used to design crystallization processes.

Further work is in progress to implement the described thermodynamic modeling in a broader simulation framework for the additional description of evaporative as well as antisolvent crystallization processes.

**Acknowledgement**

The authors thank Mrs. Jacqueline Kaufmann and Mrs. Stefanie Oberländer for their help in HPLC and PXRD measurements.

**List of symbols**

| | |
|---|---|
| $x$ | Mole fraction |
| $f$ | Fugacity (Pa) |
| $Z$ | Compressibility factor |
| $k$ | Binary interaction parameter |
| $\frac{u}{k}$ | Dispersion energy parameter (K) |
| $m$ | Segment number |
| $b$ | Interaction parameter in NRTL(J/mol) |
| $K$ | Ratio of standard fugacities |
| $X$ | Activity fraction |
| $\sigma$ | Temperature independent segment diameter (A) |
| $\kappa$ | Association volume parameter |
| $\frac{\varepsilon}{k}$ | Association energy parameter (K) |
| $\sum K_{eq}$ | Total solubility product |
| $\alpha$ | Non-randomness factor |
| $\gamma$ | Activity coefficient |
| $\tau$ | Dimensionless interaction energy parameter |

# References


[1] R. B. Gupta, R. A. Heidemann, Solubility models for amino acids and antibiotics, AIChE J. 36 (1990) 333-341. https://doi.org/10.1002/aic.690360303.

[2] K. B. Alia, H. Nadeem, I. Rasul, F. Azeem, S. Hussain, M. H. Siddique, S. Muzammil, M. Riaz, S. Nasir, Separation and purification of amino acids, in *Applications of Ion Exchange Materials in Biomedical Industries*, Springer, 2019, pp. 1-11. https://doi.org/10.1007/978-3-030-06082-4_1.

[3] L. A. Ferreira, E. A. Macedo, S. P. Pinho, Solubility of amino acids and diglycine in aqueous–alkanol solutions, Chem. Eng. Sci., 59 (2004) 3117-3124. https://doi.org/10.1016/j.ces.2004.05.001.

[4] T. NeedhamJr, A. Paruta, R. Gerraughty, Solubility of amino acids in pure solvent systems, J. Pharm. Sci., 60 (1971) 565-567. https://doi.org/10.1002/jps.2600600410

[5] M. S. Dunn, F. J. Ross, L. S. Read, The solubility of the amino acids in water, J. Biol. Chem., 103 (1933) 579-595. https://doi.org/10.1016/S0021-9258(18)75836-5.

[6] K. Hayashi, T. Matsuda, T. Takeyama, T. Hino, Solubilities studies of basic amino acids, Agric. Biol. Chem.30 (1966) 378-384. https://doi.org/10.1080/00021369.1966.10858601.

[7] E. A. Macedo, Solubility of amino acids, sugars, and proteins, Pure Appl. Chem., 77 (2005) 559–568. https://doi.org/10.1351/pac200577030559.

[8] N. A. Bowden, J. P. M. Sanders, M. E. Bruins, Solubility of the proteinogenic α-amino acids in water, ethanol, and ethanol–water mixtures, J. Chem. Eng. Data, 63 (2018) 488–497. https://doi.org/10.1021/acs.jced.7b00486.

[9] Z. Chen , R. Zhou, H. Yin, S. Yuan, 2020, Determination and correlation of temperature and pH value dependent solubility of DL-methionine, AIChE J., 66, e16270. https://doi.org/10.1002/aic.16270.

[10] X. Xu, S. P. Pinho, E. A. Macedo, Activity coefficient and solubility of amino acids in water by the modified Wilson model, Ind. Eng. Chem. Res., 43 (2004) 3200–3204. https://doi.org/10.1021/ie030860z .

[11] N. A. Bowden, D. M. Sevillano, J. P. M. Sanders, M. E. Bruins, Modelling the effects of ethanol on the solubility of the proteinogenic amino acids with the NRTL, Gude and Jouyban-Acree models, Fluid Phase Equilibr., 459 (2018) 158-169. https://doi.org/10.1016/j.fluid.2017.11.036.

[12] S. P. Pinho, C. M. Silva, E. A. Macedo, Solubility of amino acids: A group-contribution model involving phase and chemical equilibria, Ind. Eng. Chem. Res., 33 (1994) 1341-1347. https://doi.org/10.1021/ie00029a033.

[13] H. Kuramochi, H. Noritomi, D. Hoshino and K. Nagahama, Measurement of solubilities of two amino acids in water and prediction by the UNIFAC model, Biotechnol. Prog., 12 (1996) 371-379. https://doi.org/10.1021/bp960016m.

[14] P. Ji, W. Feng, Solubility of amino acids in water and aqueous solutions by the statistical associating fluid theory, Ind. Eng. Chem. Res. 47 (2008) 6275–6279. https://doi.org/10.1021/ie800313h.

[15] C. Held, L. F. Cameretti, G. Sadowski, Measuring and modeling activity coefficients in aqueous amino-acid solutions, Ind. Eng. Chem. Res., 50 (2011) 131–141. https://doi.org/10.1021/ie100088c.

[16] H. T. Do, S. Chakrabarty, C. Held, Modeling solubility of amino acids and peptides in

water and in water+2-propanol mixtures: PC-SAFT *vs.* gE models, Fluid Phase Equilibr., 542-543 (2021) 113087. https://doi.org/10.1016/j.fluid.2021.113087.
[17] J.-B. Grosse Daldrup, C. Held, F. Ruether, G. Schembecker, G. Sadowski, Measurement and modeling solubility of aqueous multisolute amino-acid solutions, Ind. Eng. Chem. Res., 49 (2010) 1395–1401. https://doi.org/10.1021/ie900913c.
[18] I. Kurosawa, A. S. Teja, R. W. Rousseau, Solid-liquid equilibria in L-leucine+L-valine+water, Fluid Phase Equilibr., 224 (2004) 245-249. https://doi.org/10.1016/j.fluid.2004.07.010.
[19] M. Prieto, Thermodynamics of solid solution-aqueous solution systems, Rev. Mineral. Geochem., 70 (2009) 2009. https://doi.org/10.2138/rmg.2009.70.2.
[20] J. Gross, G. Sadowski, Perturbed-chain SAFT: An equation of state based on a perturbation theory for chain molecules, Ind Eng Chem Res, 40 (2001) 1244-1260. https://doi.org/10.1021/ie0003887.
[21] H. Renon, J. M. Prausnitz, Local compositions in thermodynamic excess functions for liquid mixtures, AIChE J., 14 (1968) 135-144. https://doi.org/10.1002/aic.690140124.
[22] W. G. Chapman, K. E. Gubbins, G. Jackson, M. Radosz, New reference equation of state for associating liquids, Ind. Eng. Chem. Res., 29 (1990) 1709-1721. https://doi.org/10.1021/ie00104a021.
[23] J. Gross, G. Sadowski, Application of the perturbed-chain SAFT equation of state to associating systems, Ind. Eng. Chem. Res., 41 (2002) 5510-5515. https://doi.org/10.1021/ie010954d.
[24] J. M. Smith, H. C. Van Ness, M. Abbott and M. Swihart, Introduction to Chemical Engineering Thermodynamics, 8th ed., McGraw-Hill, 2018.
[25] F. Lippmann, The solubility product of complex minerals, mixed crystals and three-layer clay minerals, N. Jahrb. Mineral Abh. 130 (1977) 243-263.
[26] A. I. Isakov, E. N. Kotelnikova, S. Münzberg, S. N. Bocharov, H. Lorenz, Solid phases in the system L-valine – L-isoleucine, Cryst. Growth Des., 16 (2016) 2653–2661. https://doi.org/10.1021/acs.cgd.5b01766.
[27] A. I. Kitaigorodsky, Mixed Crystals, Springer-Verlag Berlin Heidelberg , 1984, 10.1007/978-3-642-81672-7.
[28] H. Veith, C. Luebbert and G. Sadowski, Correctly measuring and predicting solubilities of solvates, hydrates, polzmorphs, Cryst. Growth Des., 20 (2020) 723-735. https://dx.doi.org/10.1021/acs.cgd.9b01145
[29] S. Münzberg, T. G. Vu and A. Seidel-Morgenstern, Generalizing countercurrent processes: distillation and beyond, Chem. Ing. Tech., 90 (2018) 1769–1781. https://doi.org/10.1002/cite.201800132.